REPORT DOCUMENTATION PAGE

Form Approved
OMB No. 0704-0188

1. REPORT DATE *(DD-MM-YYYY)*	2. REPORT TYPE	3. DATES COVERED *(From - To)*
13-10-2014	final	Jan 2008 - June 2014

4. TITLE AND SUBTITLE

Analysis and high-resolution modeling of tropical cyclogenesis during the TCS-08 and TPARC field campaign

5a. CONTRACT NUMBER

5b. GRANT NUMBER

N00014-08-10256

5c. PROGRAM ELEMENT NUMBER

6. AUTHOR(S)

Li, Tim

5d. PROJECT NUMBER

5e. TASK NUMBER

5f. WORK UNIT NUMBER

7. PERFORMING ORGANIZATION NAME(S) AND ADDRESS(ES)

University of Hawaii at Manoa

1680 East-West Road, Honolulu, HI 96822

8. PERFORMING ORGANIZATION REPORT NUMBER

9. SPONSORING/MONITORING AGENCY NAME(S) AND ADDRESS(ES)

Marine Meteorology Program (Code 322)

Office of Naval Research

10. SPONSOR/MONITOR'S ACRONYM(S)

ONR

11. SPONSOR/MONITOR'S REPORT NUMBER(S)

12. DISTRIBUTION/AVAILABILITY STATEMENT

A distribution approved for public release; distribution is unlimited.

13. SUPPLEMENTARY NOTES

14. ABSTRACT

A number of observational and numerical modeling studies have been carried out to understand the roles of environmental flows, synoptic-scale disturbances and higher-frequency eddies in tropical cyclone formation.

15. SUBJECT TERMS

Tropical cyclogenesis, Madden-Julian Oscillation, El nino-Southern Oscillation

16. SECURITY CLASSIFICATION OF:			17. LIMITATION OF ABSTRACT	18. NUMBER OF PAGES	19a. NAME OF RESPONSIBLE PERSON
a. REPORT	b. ABSTRACT	c. THIS PAGE			19b. TELEPHONE NUMBER *(Include area code)*
			UU		

ANALYSIS AND HIGH-RESOLUTION MODELING OF TROPICAL CYCLOGENESIS DURING THE TCS-08 AND TPARC FIELD CAMPAIGN

PI: Tim Li
IPRC/SOEST, University of Hawaii at Manoa
1680 East-West Road, POST Building 409B
Honolulu, Hawaii 96822
Phone: (808) 956-9427, fax: (808) 956-9425, e-mail: timli@hawaii.edu

Co-PI: Melinda S. Peng
Naval Research Laboratory
Monterey CA 93943-5502
Phone: (831) 656-4704, fax: (831) 656-4769, e-mail: melinda.peng@nrlmry.navy.mil

Award Number: N000140810256
Period: 1 Jan 2008 – 30 June 2014

LONG-TERM GOAL

The long-term goal of this project is to improve the prediction of tropical cyclone (TC) genesis, structure and intensity changes through improved understanding of the fundamental mechanisms involved. The accurate prediction of TC genesis, structure and intensity changes is critical to Navy missions and civilian activities in coastal areas. Significant gains have been made in the TC track prediction over the past decades. The genesis and intensity forecast, however, has shown very little progress during the same period. A main factor contributing to the lack of skill in the prediction of TC genesis and intensity is the lack of observations prior to and during TC genesis and intensification periods and the inadequate understanding of physical mechanisms that control the cyclogenesis and intensity change. The TCS-08 and TPARC field campaign provide an unprecedented opportunity for us to gain the first-hand insight of observed characteristics of TC genesis in western Pacific and to compare them with high-resolution model simulations. By analyzing and assimilating these data, we intend to understand the physical mechanisms that involve the TC internal dynamic and thermodynamic processes, external forcing, and scale interactions. Only after thoroughly understanding these processes, can one be able to tackle the weaknesses in the current state-of-art weather forecast models.

OBJECTIVE

The objective of this project is to investigate the synoptic and climatic aspects of tropical cyclone (TC) genesis in the western North Pacific (WNP). On one hand, specific synoptic and dynamic processes through which an initial weak vortex (either mid-level or near-bottom vortex) develops into a TC will be investigated in a cloud-resolving model. On the other hand, the large-scale control of the Madden-Julian Oscillation (MJO) and El Nino-Southern Oscillation (ENSO) on TC genesis in the WNP will be examined. Additional effort is to conduct data assimilation using data collected from TCS-08 observational campaign. We will examine how the cyclogenesis forecast may be significantly improved with a better description of the dynamic and thermodynamic precursor signals.

APPROACH

For understanding the synoptic and dynamic aspects of cyclogenesis, a multi-nested WRF model (with 2 km resolution in the innermost mesh) will be used to simulate both idealized and real-case cyclogenesis events. Through the diagnosis of the model outputs, we intend to understand the common and different development characteristics associated with cyclogenesis in an environment with a near bottom vortex (EBV) and an environment with a mid-level vortex (EMV). The genesis time for each model run will be defined based on an objective way. A concept of the cyclogenesis efficiency (which is related to the initial environmental dynamic and thermodynamic conditions) will be introduced. A number of idealized experiments will be designed to illustrate the relative importance of initial column-integrated absolute vorticity, PBL parameters, surface fluxes, and vertically integrated relative humidity in determining the TC genesis efficiency.

For understanding the climatic aspect of cyclogenesis, various statistical tools such as the wavenumber-frequency analysis, lagged regression analysis, and composite analysis methods will be applied to understand the role of the MJO and ENSO in determining the intraseasonal and interannual variability of TC activity in the WNP.

For the data assimilation task, WRF 3DVar assimilation system will be employed. Because the TCS-08 campaign provides variety types of in-situ data at irregular spatial and temporal intervals, we intend to construct a high-resolution regular-grid reanalysis product that combines in-situ observations (such as ELDORA radar, Doppler wind lidar, dropsondes and driftsondes) with satellite remote sensing products.

WORK COMPLETED

Twenty-nine papers relevant to tropical cyclone genesis and tropical wave dynamics/multi-scale interactions were published in professionally referred journals. In the following we highlight some results.

MAJOR RESULTS

1. Simulations of cyclone genesis associated with Rossby wave energy dispersion of a pre-existing typhoon

A real-case TC genesis event of Typhoon Prapiroon (2000) in WNP was simulated using WRF. This genesis is associated with Rossby wave energy dispersion of a pre-existing TC Bilis (2000). Using the reanalysis data as an initial condition, we successfully simulated this cyclogenesis event 3 days prior to the formation of Prapiroon. The simulated Rossby wave train bears many similarities as those from the observed (see Fig. 1). For example, the wavelength of the Rossby wave train is about 2500 km, and the vertical structure shows a baroclinic structure along the axis of the wave train. In addition to low levels, a significant wave train with alternating positive and negative vorticity perturbations appears at 200 hPa. The upper level flow is characterized by an intense asymmetric outflow jet.

Two sensitivity experiments are conducted to confirm the role of the Rossby wave energy dispersion from the pre-existing TC. In a control experiment (CTL), we retain both the pre-existing TC Bilis and its wave train in the model initial condition. In a sensitivity experiment (EXP), we remove the pre-existing TC Bilis while keeping its wave train. The numerical simulations demonstrated the important role of the pre-existing TC energy dispersion in the subsequent TC genesis. Based on the model diagnosis, we propose that both a direct and indirect processes are involved. The direct process is through the TC southeastward energy dispersion, by which the induces Rossby wave train triggers the convection-circulation feedback. The indirect process is through the upper tropospheric influence associated with the asymmetric outflow jet. On one hand, the outflow jet extends horizontally and enhances the divergence (convergence) tendency to the left (right)-exit of the jet due to weak inertial stability. The upper-level divergence superposing on the low-level cyclogenesis area may boost vigorous convective activities (Fig. 2). The prolific meso-scale vortices concentrate in the cyclonic vorticity region, which helps create a primary vortex through vortex merging and the absorption of the vorticity of the convectively generated vortices, and thus favors TC-scale vortex development. On the other hand, the asymmetric outflow

jet induces a well-organized cyclonic eddy momentum flux, which acts to drive the radial circulation and accelerates the growth of a new TC.

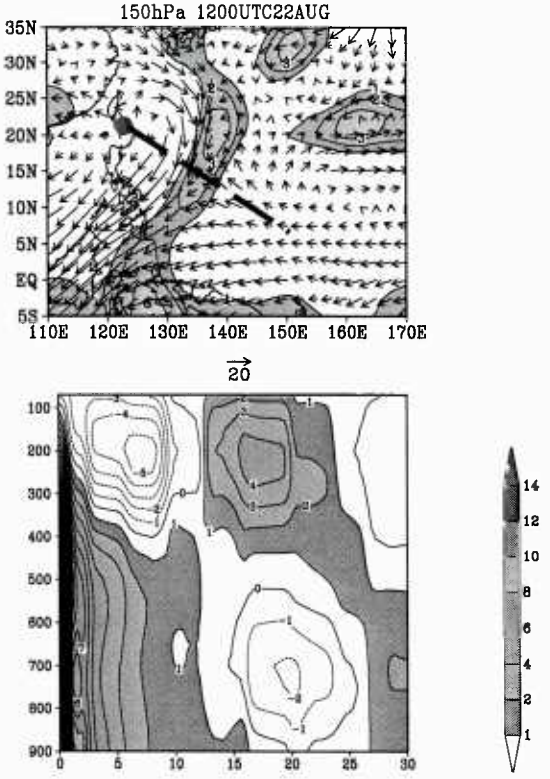

Fig. 1 The observed 150-hPa wind vector (m s^{-1}) and relative vorticity (unit: 10^{-5} s^{-1}) fields at 1200 UTC 22 August 2000 (top panel), and the vertical-radius cross-section of relative vorticity fields (bottom panel) along a northwest-southeast oriented axis (the dashed line).

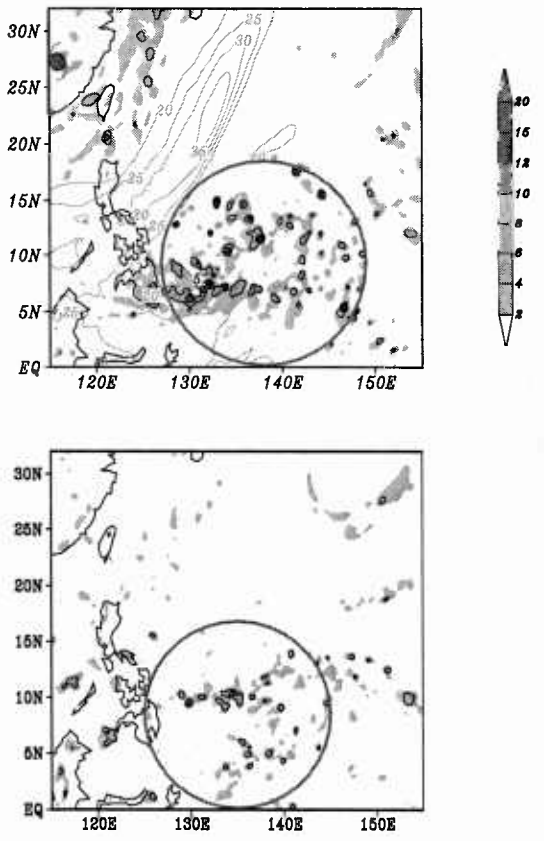

Fig. 2 The upper-level divergence ($\geq 2\times10^{-5}$ s^{-1} are shaded) and wind (contour interval: 5 m s^{-1}) fields at the jet core region in CTL (top panel) and EXP (bottom panel) at 1200UTC 24 August.

2. Tropical cyclone genesis efficiency: Mid-level versus bottom vortex

Cloud resolving WRF model is used to investigate the tropical cyclone genesis efficiency in an environment with a near bottom vortex or an environment with a mid-level vortex. Five experiments were designed with different initial vertical vorticity and moisture profiles. In the first experiment (MID_VORTEX), we mimic a mid-level precursor condition, by specifying an initial cyclonic vortex that has a maximum vorticity at 600 hPa and corresponds to a maximum wind speed of 8 m s^{-1} at a radius of 100 km and a size of 500 km radius where the wind vanishes. The vorticity gradually decreases both upward and downward, and vanishes at the surface. In the second experiment (BTM_VORTEX), an initial maximum precursor perturbation with a maximum wind speed of 8 ms^{-1} is located at the surface. Figures 1a and 1b show the vertical-radial cross section of the tangential wind of these initial vortexes. The third

and the fourth experiment contain a shallow mid-level vortex (SHAL_MID) and a shallow bottom vortex (SHAL_BTM), respectively, to identify the PBL effects and to better separate the mid-level and bottom vortices. Their vertical wind profiles are shown in Figs. 3c and 3d. The fifth experiment (MOIST) has the vortex profile as the MID_VORTEX except with a greater moisture to investigate the dependence of TC genesis efficiency on the humidity profile.

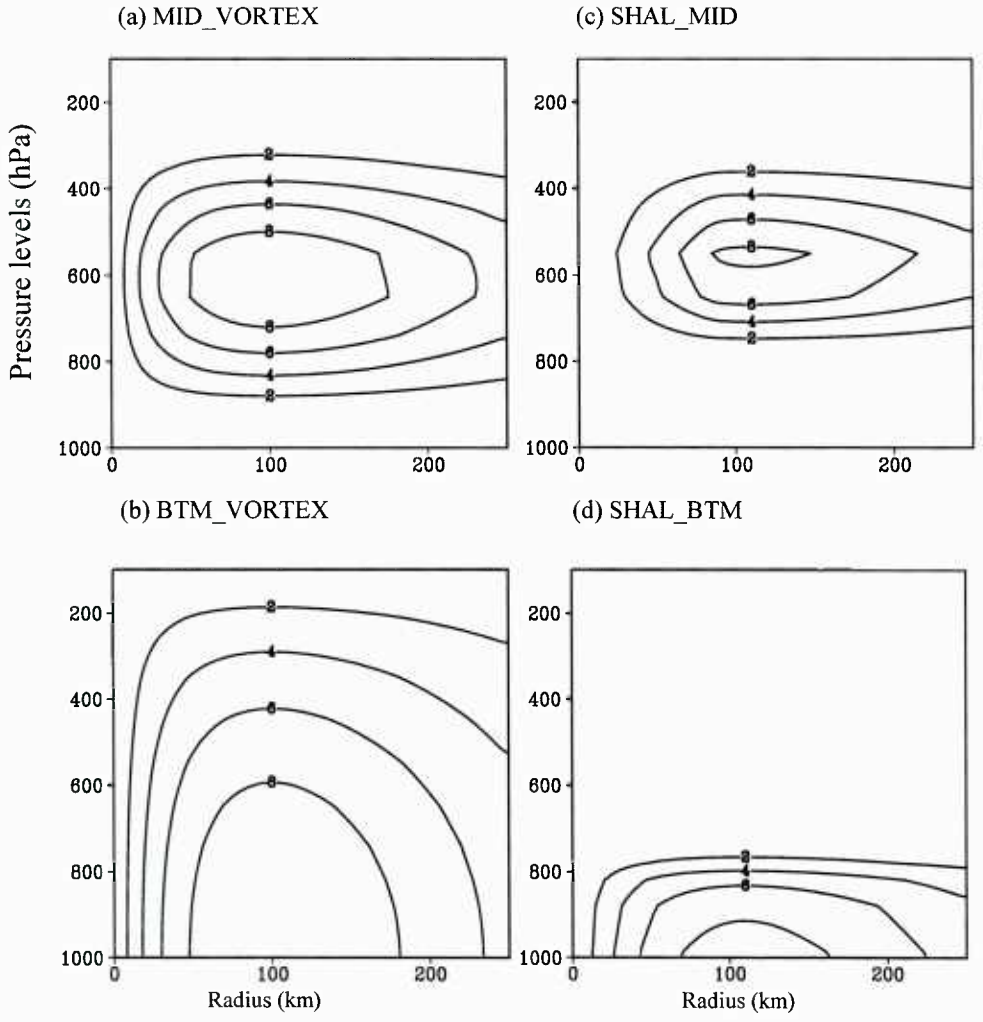

Fig. 3 The vertical-radial cross section of tangential velocity (ms^{-1}) of the initial vortex in (a) MID_VORTEX, (b) BTM_VORTEX, (c) SHAL_MID and (d) SHAL_BTM.

All experiments above are able to develop a realistic and similar tropical cyclone, although the time taken is different. These time differences represent the genesis efficiency of the initial setup of the precursor vortex or the environmental moisture

profile. It is found that all experiments share the following development characteristics: 1) a transition from non-organized cumulus-scale (~5 km) convective cells into an organized meso-vortex-scale (~50 km) system through upscale cascade and system scale intensification (SSI) processes, 2) the establishment of a nearly saturated air column prior to a rapid drop of the central minimum pressure, and 3) a convective-stratiform phase transition.

The numerical experiments above show that the genesis timing depends crucially on the initial vertical moisture and vorticity profiles. Based on these experiments and following the formula of the genesis potential index by Emanuel and Nolan (2004), we introduce a genesis efficiency index (GEI) to quantify the impact of initial vorticity and moisture profiles on the cyclogenesis. The key parameters in the GEI include the column integrated (1000-200hPa) absolute vorticity, relative vorticity at top of the planetary boundary layer (PBL), and vertically integrated (1000-500hPa) relative humidity (RH). Figure 4 shows that the GEI presents well the model simulated genesis feature. We found that with a similar column integrated (1000-200hPa) absolute vorticity, a bottom precursor vortex has a higher genesis efficiency than a mid-level vortex.

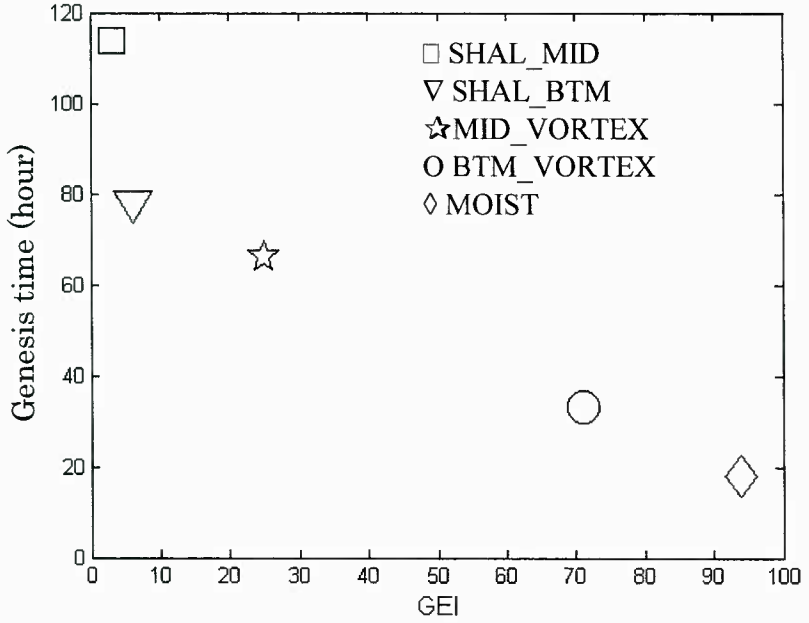

Fig. 4 Relationship between the GEI and the genesis time in the five experiments.

A salient feature among all five experiments above is a close relationship between the deepening of a moist layer and cyclogenesis time. For instance, in MID_VORTEX, there is a steady increase of the moist layer in the core region during hour 24-60. The

90% RH layer thickens from 900 hPa at hour 24 to about 500 hPa at hour 60. It is the establishment of this near-saturation air column that signifies the next development stage: deepening of cyclonic vorticity and a rapid drop of minimum sea level pressure. In all five experiments above, the genesis time occurs shortly after a near-saturated air column is set up. This preconditioning of the deep moist layer in the core region was also found in Nolan (2007) with different model physics. Figure 5 illustrates the evolution of the vertically (1000-500 hPa) integrated RH averaged in the core region (within a 100km x 100km domain) and its relationship with the TC genesis. In all five experiments, the genesis start shortly after the column averaged RH reaching 90%, confirming that the establishment of a near-saturated deep air column is indeed a precondition for cyclogenesis.

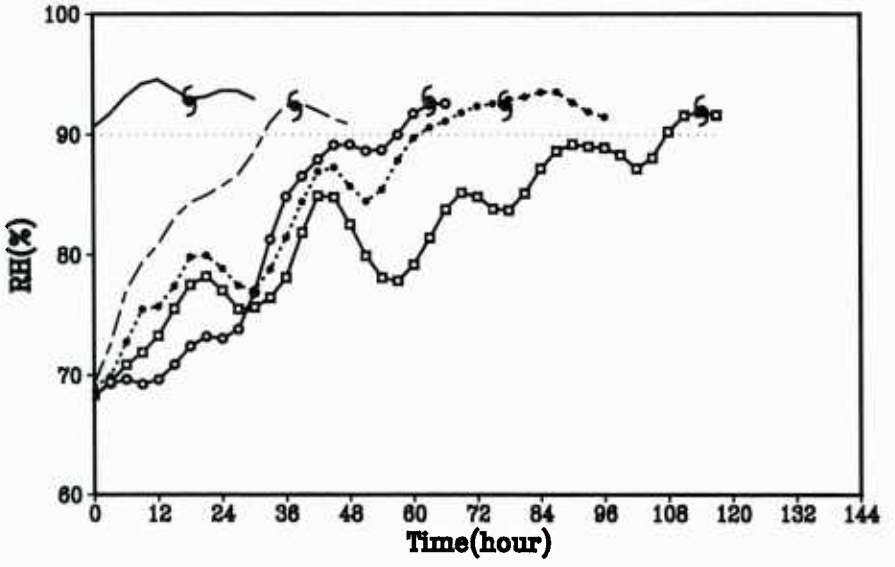

Fig. 5 Time evolution of the column averaged $\overline{RH}$ (from the surface to 500hPa) in MOIST (solid line), BTM_VORTEX (long dashed line), MID_VORTEX (solid line with open circle), SHAL_BTM (dotted line with solid circle), SHAL_MID (solid line with open square), respectively. The hurricane symbols represent the genesis time of each experiment.

3. Factors that affect multiple tropical cyclone formation

The statistical feature of occurrence of summer (June-September) multiple tropical cyclone (MTC) events in the western North Pacific was examined for the period of 1979-2006 (Gao and Li 2011). The number of MTC events ranged from 1 to 8 per year, experiencing a marked interannual variation. The spatial distance between the TCs associated with MTC events is mostly less than 3000 km, which accounts for 73% of

total samples. The longest active phase of a MTC event lasts for nine days, and about 80% of the MTC events last for five days or less.

A composite analysis of active and inactive MTC phases reveals that positive low-level (negative upper-level) vorticity anomalies and enhanced convection and mid-tropospheric relative humidity are the favorable large-scale conditions for MTC genesis. It is noted that the MTC events are closely associated with the Madden-Julian Oscillation (MJO) and the biweekly (10-20-day) oscillation (BWO). Figure 1 shows the composites of 25-70-day band-pass filtered OLR fields during the MTC inactive and active phase respectively. Note that during the MTC active phase, negative OLR anomalies associated with the MJO cover the entire SCS/WNP region from 110°E to the east of 170 °E and from 5°N to 25°N. The condition is completely reverse in the MTC inactive phase, in which positive intraseasonal OLR anomalies occupy the region. The difference is statistically significant, exceeding the 95% confidence level. This indicates that the MJO is in a wet (dry) phase with enhanced (suppressed) convective activity in WNP when an active (inactive) MTC phase occurs. This implies that the large-scale circulation anomaly associated with MJO favors the genesis of MTC events.

The BWO, on the other hand, shows a different spatial pattern (Fig. 6). It is found that during the MTC active phase a negative OLR anomaly appears west of 140 °E, while a positive OLR anomaly occurs to the east. The negative OLR anomaly to the west is stronger than the positive one to the east. Such a zonal dipole pattern is consistent with the fact that the BWO has a relatively short zonal wavelength compared to that of the MJO. An approximately opposite pattern of the OLR anomaly appears in the inactive MTC composite. The difference is most significant in a region from 125°E to 140°E. The result suggests that the strengthened BWO activity in that region favors the MTC generation in the WNP.

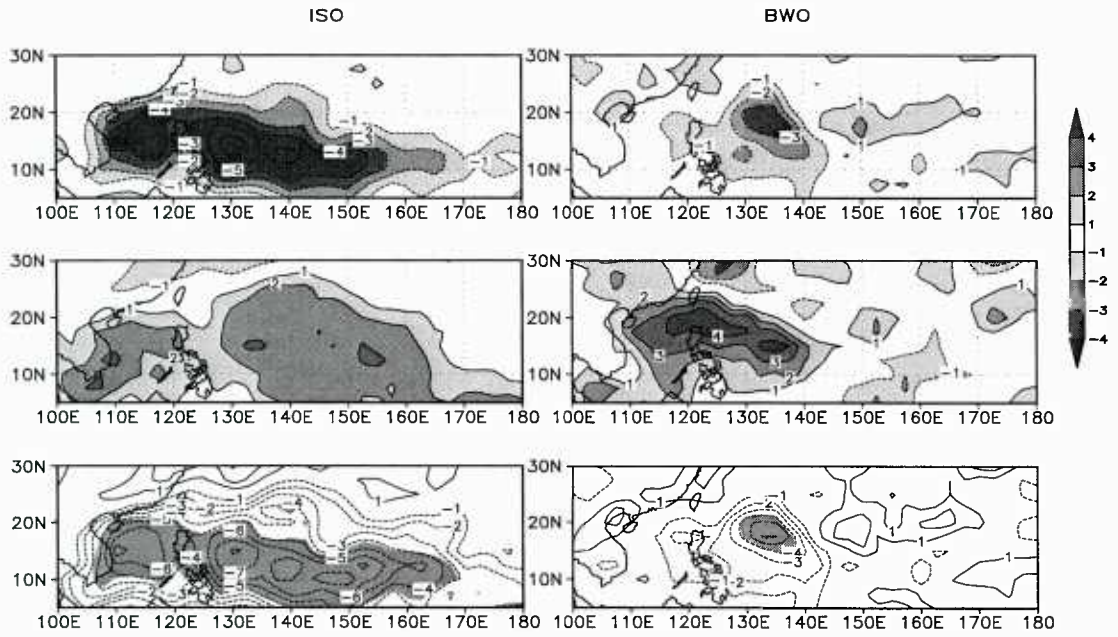

Figure 6 The 25-70-day (left) and 10-20-day (right) band-pass filtered OLR (unit: W/m^2) fields composed based on MTC active (top panel) and inactive (middle panel) phases and their difference fields (bottom panel). The OLR anomalies with a value greater than 1 W/m^2 or less than -1 W/m^2 are shaded in top and middle panels. Shading in the bottom panel indicates that the difference between the active and inactive phase exceeds a 95% confidence level.

The possible effect of the large-scale control of the MJO and BWO may be revealed by counting the percentage of individual MTC events that appear during the active phases of the MJO and BWO respectively. Due to the spatial variability of cyclogenesis locations associated with the MTC events, the OLR values associated with the MJO and BWO at individual genesis locations on the genesis dates were calculated. Prior to that, a Lanczos filter is applied to the daily OLR field to extract the biweekly (10-20-day), intraseasonal (25-70-day) and lower frequency (> 90 days) components. The number of positive and negative OLR values was then counted at each of the genesis location and date for each of the following scenarios: the MJO mode only, the BWO mode only, sum of the MJO and BWO modes, and sum of the MJO, BWO and lower-frequency oscillation (LFO, >90 days) modes.

Table 1 shows the percentage of number of the negative OLR values during active MTC events for each of the scenarios above. It is found that about 77% of the TCs associated with the active MTC events occur when either BWO or MJO is in a wet phase. The combination of the BWO and MJO modes leads an increase of the occurrence percentage to 84%. This implies that the predictability of the MTC events might increase when one considers both the MJO and BWO impacts. The percentage of

occurrence of the MTC events increases further to 98% when the combined BWO, MJO and LFO forcing effects are included.

Table 1. The percentage of occurrence of the MTC events in the genesis locations where the BWO, MJO and/or LFO are in a wet phase

Mode	**Percentage of occurrence of negative OLR values**
BWO (10-20-day)	77.30
MJO (25-70-day)	76.69
BWO + MJO	84.05
BWO + MJO + LFO	97.85

The observational analysis result above indicates that the occurrence of the MTC events is greatly regulated by the combined large-scale impacts of the BWO, MJO and the lower-frequency oscillation. On the interannual timescale, the MTC frequency is closely related to the seasonal mean anomalies of 850-hPa vorticity, OLR and 500-hPa humidity fields. The MJO and BWO activity is greatly strengthened (weakened) in the WNP region during the MTC active (inactive) years.

4. Impacts of two types of El Niños on tropical cyclone tracks

Impacts of two types of El Niños, the eastern Pacific El Niño (EP-EN) and the central Pacific El Niño (CP-EN), on tropical cyclone (TC) tracks over the western North Pacific (WNP) were examined based on observational data (Hong et al. 2011). Whereas TC tracks between CP-EN and EP-EN show a small difference in boreal summer (JJA), they do exhibit a great difference in boreal autumn (SON), that is, TCs recurve northward at a further westward location near the coastline of East Asia during CP-EN. As a consequence, more TCs make landfall to Taiwan and South China during CP-EN. A further observational analysis indicates that the westward shift of the subtropical high and associated steering flow during CP-EN is a key factor that causes the difference in the TC tracks in autumn. Numerical experiments further suggest that the difference of local SST in the WNP between CP-EN and EP-EN accounts for the distinctive differences in the local Hadley circulation, the subtropical high and the TC steering flow.

5. Bimodal character of cyclone climatology in Bay of Bengal

The annual cycle of tropical cyclone (TC) frequency over the Bay of Bengal (BoB) exhibits a notable bimodal character, different from a single peak in other basins. The monthly occurrence number of TCs based on JTWC best track data in seven major TC active regions is shown in Fig. 7. Consistent with previous studies, there is a marked difference in the TC genesis frequency between the BoB and other ocean basins. TC frequency in the BoB has two peaks in monsoon transition periods (April-May and October-November), while very low genesis frequency occurs during the strong southwest monsoon period (June-July-August-September).

Previous studies suggested that the bimodal feature of TC frequency in the BoB and AS is attributed to the annual cycle of the background vertical shear as strong vertical shear in boreal summer prevents TC formation. Here we will develop a quantitative diagnosis method to reveal the relative roles of large-scale environmental factors in causing the bimodal feature. Using the NCEP monthly reanalysis data for 1981-2009, we calculate the box-averaged climatologic monthly GPIs in seven regions. The size of each box is defined as follows: (10-20°N, 67-75°E) for the AS, (5-15°N, 80-95°E) for the BoB, (5-20°N, 130-150°E) for the WNP, (10-20°N, 240-260°E) for the ENP, (10-20°N, 310-340°E) for the NATL, (10-25°S, 55-100°E) for the SIO and (10-25°S, 160°E -170°W) for the SWP. As shown in Fig. 2, the GPI index well captures the annual cycle pattern in all regions, especially the double peaks in the BoB.

Figure 7 shows that GPI represents well the combined effect of the four large-scale environmental processes on the cyclone genesis. A methodology was developed to quantitatively assess the relative contributions of four environmental parameters. Different from a conventional view that the seasonal change of vertical shear causes the bimodal feature, we found that the strengthened vertical shear alone from boreal spring to summer cannot overcome the relative humidity effect. It is the combined vertical shear, vorticity and SST that leads to the GPI minimum in boreal summer. It is noted that TC frequency in October-November is higher than that in April-May, which is primarily attributed to the difference of mean relative humidity between the two periods. In contrast, more super cyclones (Category 4 or above) occur in April-May than in October-November. It is argued that greater ocean heat content, the first branch of northward propagating intra-seasonal oscillations (ISOs) associated with the monsoon onset over the BoB, and stronger ISO intensity in April-May are favorable environmental conditions for cyclone intensification.

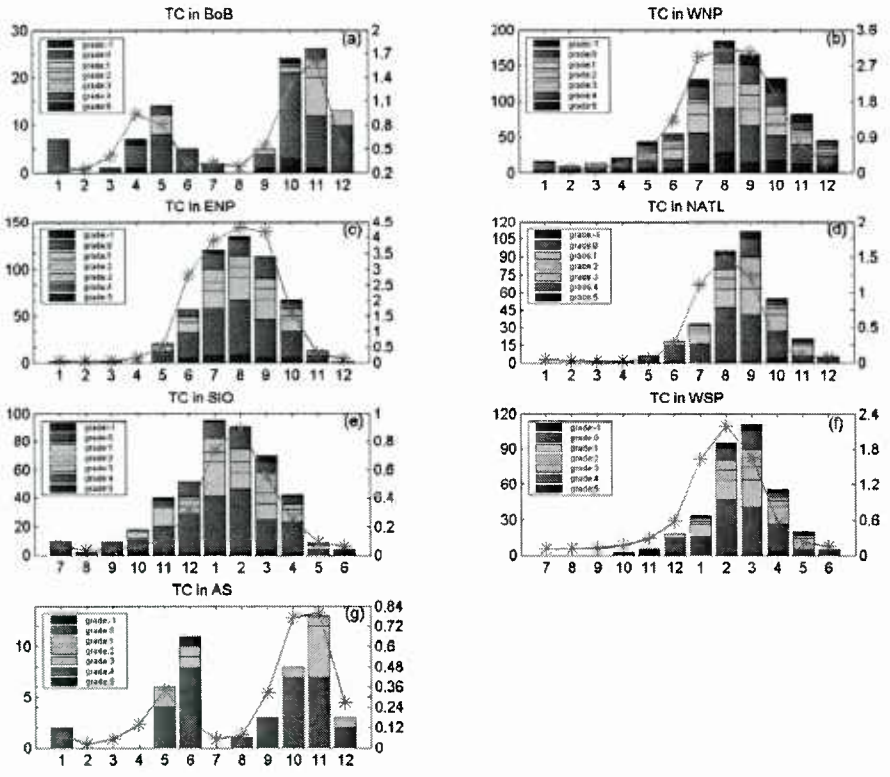

Fig. 7 Monthly TC numbers (column) during 1981-2009 in the (a) BoB, (b) WNP, (c) ENP, (d) NATL, (e) SIO and (f) WSP, respectively. According to Saffir-Simpson scale, grades -1 and 0 denote tropical depression and tropical storm, and grade 1 to 5 represents different typhoon strength, ranged from category 1 to category 5, as the legend shows. The overlaid gray curves represent the climatologic monthly GPI values. The left vertical-axis is for TC number and the right vertical-axis is for the GPI value.

6. Interannual Variation of Multiple Tropical Cyclone Events in the Western Pacific

The interannual variability of occurrence of multiple tropical cyclone (MTC) events during June-October in the western North Pacific is examined for the period of 1979-2006. It is found that the number of the MTC events is ranged from 2 to 9 per year, exhibiting a remarkable year-to-year variation. Seven active and seven inactive MTC years are identified. Compared to the inactive years, TC genesis locations are extended further to the east and in the meridional direction during the active MTC years. A composite analysis shows that the MTC inactive years are often associated with the El Niño decaying phase, as warm SST anomalies in the equatorial eastern-central Pacific in the preceding winter transition into cold SST anomalies in the concurrent summer.

Associated with the SST evolution are suppressed low-level cyclonic vorticity and weakened convection in the WNP monsoon region.

In addition to the mean flow difference, significant differences between the active and inactive MTC years are also found in the strength of the atmospheric intraseasonal oscillation (ISO). Compared to the inactive MTC years, ISO activity is greatly strengthened along the equator and in the WNP region during the active MTC years. Both westward and northward propagating ISO spectrums are strengthened during the MTC active years compared to those during the inactive years. The combined mean state and ISO activity changes may set up a favorable environmental condition for the generation of the MTC events.

7. Characteristics of tropical cyclone genesis in the western North Pacific during the developing and decaying phases of two types of El Niño

During the developing phase of central Pacific El Nino (CPEN), more frequent TC genesis over the northwest quadrant of the western North Pacific (WNP) is attributed to the horizontal shift of environmental vorticity field. Such a northwestward shift resembles the La Niña composite, even though factors that cause the shift differ (in the La Niña case the relative humidity effect is crucial). Greater reduction of TC frequency happened during the decaying phase of eastern Pacific El Nino than CPEN, due to the difference of the anomalous Philippine Sea anticyclone strength. The TC genesis also exhibits an upward (downward) trend over the northern (southern) part of the WNP, which is linked to regional circulation and SST changes.

8. Effects of vertical shears and mid-level dry air on tropical cyclone developments

A set of idealized experiments using WRF are designed to investigate the impacts of mid-level dry air layer, a vertical shear, and their combined effects, on tropical cyclone (TC) developments. We design the following numerical experiments. In the control experiment (NOSH_CTL), we exclude both the dry air intrusion and the vertical shear. The initial fields contain a weak symmetric cyclonic vortex, with a maximum surface wind speed of 8 ms^{-1} at a radius of 150 km and the wind speed decreasing with height. This control experiment represents TC development under the favorable conditions with no vertical shear or a dry air layer. The second experiment (NOSH_DRY) is designed to examine the impact of the mid-level dry air layer with no mean flow. The specification of dry air layer follows Braun et al. (2012). A dry air layer is specified between 850 and 650 hPa, in which RH is set as 25% to mimic the dry SAL. This dry

air layer is embedded at all grid points 150-km north of the initial vortex center. Four additional experiments with different vertical shears are designed. WSH_CTL and ESH_CTL are to examine the impact of different vertical shear profiles on TC development without mid-level dry air layer. In the flow with an easterly (westerly) wind shear, the zonal wind decreases (increases) linearly from 4 (-4 ms^{-1}) at the surface to -4 (4ms^{-1}) at the top of the model, and zero wind speed at 500 hPa. WSH_DRY and ESH_DRY have the same shear as in WSH_CTL and ESH_CTL, but with dry air located to the north of the vortex.

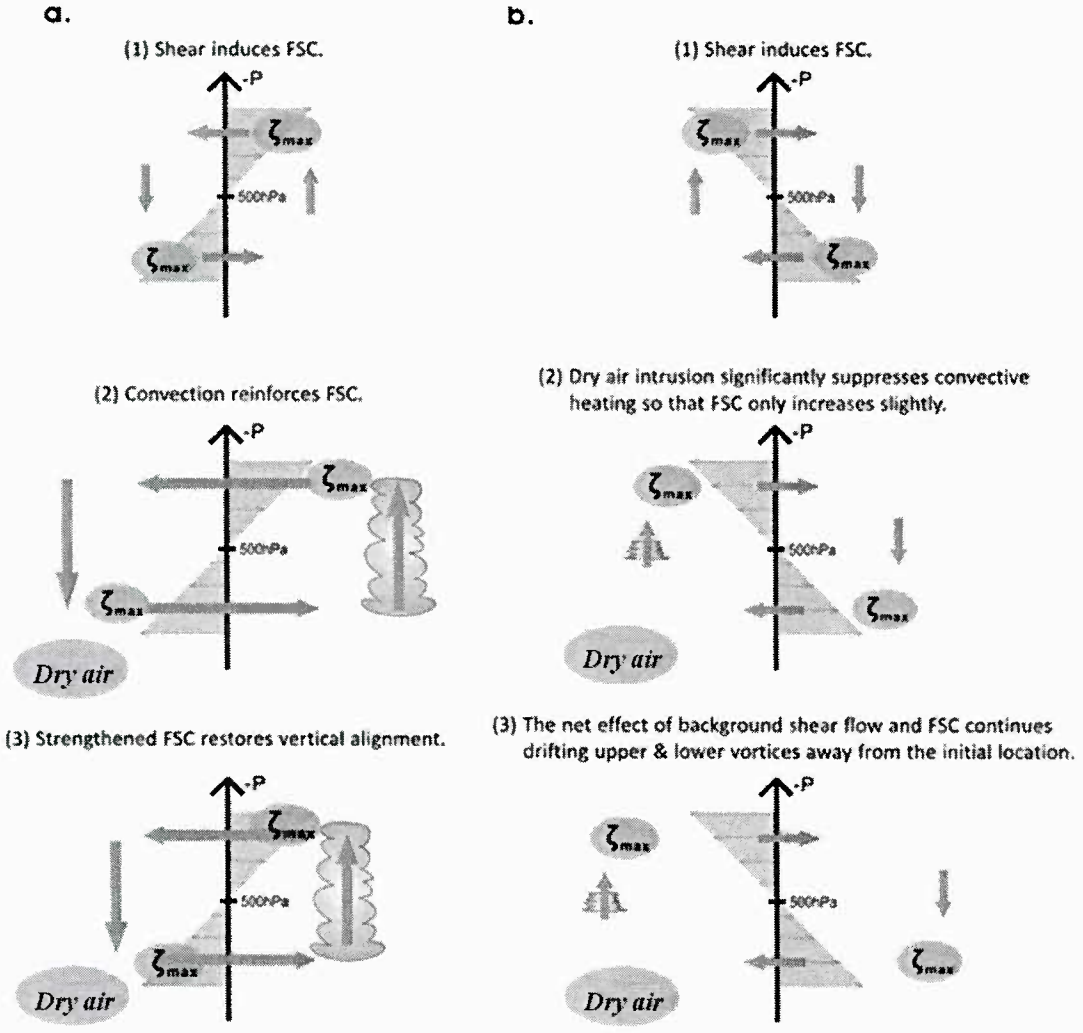

Fig. 8 Schematic summarizing the effect of FSC on the impact of vertical shear: (a) how the shear induced FSC is established and how the convection reinforced FSC helps restore the vertical alignment in WSH_DRY and (b) how the FSC fails to offset the shear advective effect due to dry air intrusion in ESH_DRY.

Numerical simulations show that without the existence of a mid-level dry air, the easterly and westerly shear effects on a TC development are quite similar. However, in the presence of dry air, the intensification rate and the final TC state in WSH_DRY and ESH_DRY are very different from each other. In ESH_DRY, dry air is quickly wrapped into the vortex core region during the first 48 hours, and covers almost the entire core region by 96 hour. As a consequence, there is no TC genesis. In contrast, in WSH_DRY, a TC is able to form, even though its intensification rate is weaker than that in WSH_CTL. The results indicate that the mid-level dry air imposed is very effective in hindering the storm development under the shear condition. The impact of dry air is highly sensitive to the orientation of vertical shear.

Why does the dry air allow the TC development under the westerly shear but not the easterly shear? We hypothesize that the difference is attributed to the relative location of dry air in relevance to the downshear quadrant. When it is placed to the right (left) of the downshear region, the dry air is easier (not easier) to be advected into the convective region of the FSC. Figure 8 contains two schematic diagrams showing how the westerly and easterly shear affect the FSC and the subsequent vertical alignment process in the case when the dry air is placed initially to the north of the vortex center. In the westerly shear case (Fig. 8a), a cyclonic vortex that is initially vertically aligned will gradually tilt eastward with height due to vorticity advection. While the upper-level vortex shifts eastward from the original position, the lower-level vortex shifts westward. According to the omega equation, positive (negative) vorticity advection to the east of the upper (lower) level vorticity maximum would lead to ascending motion. Likewise, the differential vorticity advection will lead to descending motion to the west side of the low-level circulations. Thus a secondary circulation (green arrows) forms, with maximum vertical velocity near 500 hPa. With the aid of the moist process, the ascending branch of the FSC is strengthened due to condensational heating associated with enhanced convection. Therefore, the FSC is reinforced to help overcome the shear-induced drifting and "restore" the vertical alignment.

How does the ESH_DRY differ from the WSH_DRY? Recalled that in our model configurations, the dry air layer is place to the north of the vortex center. Due to the combination of cyclonic circulation of the vortex and the mean flow, the dry air originally located north of the vortex will be quickly advected to the west side of the circulation. As a result, there is an asymmetry of the moisture distribution in the zonal direction with dryer air to the west and moister air to the east. While the FSC for the easterly shear (upper panel in Fig. 8b) is exactly opposite to the one for the westerly shear (upper panel in Fig. 8a), the dry-air zonal asymmetric distribution comes to play in the next step. As illustrated in the middle panel of Fig. 8b for ESH_DRY, with the

dryer air existing in region where the upward branch of the FSC resides, the FSC in ESH_DRY lacks convective mechanism for enhancing itself as seen in the WSH_DRY case. Therefore, the parted upper-level vortex due to the shear continues drifting away from the low-level vortex.

This study indicates the importance of dry air and vertical shear orientations in determining the impact. The background vertical shear causes the tilting of an initially vertically aligned vortex. The shear forces a secondary circulation (FSC) with ascent (descent) in the downshear (up-shear) flank. Hence, convection tends to be favored on the downshear side. The FSC reinforced by the convective heating may overcome the shear-induced drifting and "restore" the vertical alignment. When dry air is located in the downshear right quadrant of the initial vortex, the dry advection by cyclonic circulation brings the dry air to the downshear side and suppresses moist convection therein. Such a process disrupts the "restoring" mechanism associated with the FSC and thus inhibits TC development. The sensitivity experiments show that, for a fixed dry air condition, a marked difference occurs in TC development between an easterly and a westerly shear background.

9. Tropical cyclogenesis in the western North Pacific as revealed by the 2008-2009 YOTC data

The Year of Tropical Convection (YOTC) high-resolution global reanalysis data were analyzed to reveal precursor synoptic-scale disturbances related to tropical cyclone (TC) genesis in the western North Pacific (WNP) during 2008-2009 typhoon seasons. A time filtering is applied to the data to isolate synoptic (3-10-day), quasi-biweekly (10-20-day) and intraseasonal (20-90-day) time-scale components. The results show that four types of precursor synoptic disturbances associated with TC genesis can be identified in the YOTC data. They are 1) Rossby wave trains associated with pre-existing TC energy dispersion (TCED) (24%), 2) synoptic wave trains (SWT) unrelated to TCED (32%), 3) easterly waves (EW) (16%), and 4) a combination of either TCED-EW or SWT-EW (24%). The percentage of identifiable genesis events is higher than previous analyses.

Most of the genesis events occurred when atmospheric quasi-biweekly and intraseasonal oscillations are in an active phase, suggesting a large-scale control of low frequency oscillations on TC formation in the WNP. For genesis events associated with SWT and EW, maximum vorticity was confined in the lower troposphere. During the formation of Jangmi (2008), maximum Rossby wave energy dispersion appeared in middle troposphere. This differs from other TCED cases in which energy dispersion is

strongest at low level. As a result, the mid-level vortex as a result of Rossby wave energy dispersion grew faster during the initial development stage of Jangmi.

10. Dependence of tropical wave activity on ENSO phase

The three-dimensional structure and evolution characteristics of tropical depression (TD) and mixed Rossby-gravity wave (MRG) type disturbances in the tropical western North Pacific (WNP) during El Niño and La Niña summers are investigated based on observational and reanalysis data. A clear MRG-to-TD transition was observed during El Niño summers while such a transition is unclear during La Niña summers. The vertical structure of the TD-MRG waves appears equivalent barotropic during El Niño but becomes tilted eastward with height during La Niña. The diagnosis of barotropic energy conversion shows that both the rotational and divergent components of the background flow change associated with ENSO are responsible for energy conversion from the mean flow to the TD-MRG perturbations.

A further examination of the pure MRG mode shows that its intensity does not vary between El Niño and La Niña while its phase speed does. A faster (slower) westward propagation speed during La Niña (El Niña) is attributed to enhanced (reduced) mean easterlies in the western equatorial Pacific. The heating associated with the MRG wave appears more anti-symmetric during La Niña than during El Niño. In contrast to the MRG waves, the amplitude of the TD waves depends greatly on the ENSO phase. The enhanced (suppressed) TD disturbances during El Niño (La Niña) is attributed to greater (less) barotropic energy conversion associated with the background flow change. The vertical structure of the TD waves appears quasi-barotropic in the geopotential height field but baroclinic in the divergence field.

IMPACT/APPLICATIONS

The investigation of dependence of TC genesis efficiency on initial vortex structure and large-scale factors that control TC genesis and the construction of the typhoon reanalysis product may improve our current understanding of cyclogenesis dynamics and promote a more skillful prediction of TC genesis and intensity change.

TRANSITIONS

Results from this study may lead to improvement of TC prediction in the NOGAPS and COAMPS models. The TC dynamic initialization scheme used in the typhoon reanalysis effort may be transitioned into a 6.4 project.

RELATED PROJECTS

This project is complimentary to the ONR funding entitled "Initialization of tropical cyclone structure for operational application" in which we applied TC dynamic initialization strategy to the Observation System Simulation Experiment (OSSE) in an idealized setting using the WRF model and real-case TC forecast during 2009-2010 using NRL COAMPS-TC model. Knowledge gained from this project will help improve the current operational model TC initialization.

PUBLICATIONS

The following are papers that are fully or partially supported by this ONR grant:

1. Cao, X., T. Li, M. Peng, W. Chen, and G. Chen, 2014: Effects of the monsoon trough interannual variation on tropical cyclogenesis over the western North Pacific. *Geophy. Res. Lett.*, in press.
2. Xu, Y., T. Li, and M. Peng, 2014: Roles of Synoptic-scale Wave Train, Intraseasonal Oscillation, and High-frequency Eddies in Genesis of Typhoon Manyi (2001). *J. Atmos. Sci.*, in press.
3. Murakami, H., P.-C. Hsu, O. Arakawa, and T. Li, 2014: Influence of model biases on projected future changes in tropical cyclone frequency of occurrence. *J. Climate*, 27, 2159-2181.
4. Chung, P.-H., and T. Li, 2014: Characteristics of tropical cyclone genesis in the western North Pacific during the developing and decaying phases of two types of El Niño, *Journal of Tropical Meteorology*, in press.
5. Wu, L., Z. Wen, T. Li, and R. Huang, 2014: ENSO-phase dependent TD and MRG wave activity in the western North Pacific. *Climate Dynamics*, 42, 1217-1227.
6. Murakami, H., T. Li, and M. Peng, 2013: Changes to Environmental Parameters that Control Tropical Cyclone Genesis under Global Warming. *Geophy. Res. Lett.*, **40** (10), 2265-2270.
7. Murakami, H., B. Wang, T. Li, and A. Kitoh, 2013: Projected future increase in tropical cyclones near Hawaii. *Nature Climate Change*, **3**, 749-754.

8. Hendricks, E.A., M. S. Peng, and T. Li, 2013: Evaluation of multiple dynamic initialization schemes for tropical cyclone prediction. *Mon. Wea. Rev.*, 141, 4028-4048.
9. Ge, X., T. Li, and M. Peng, 2013: Effects of vertical shears and mid-level dry air on tropical cyclone developments. *J. Atmos. Sci.*, 70(12), 3859-3875.
10. Li, Z., W. Yu, T. Li, V. S. N. Murty, and F. Tangang, 2013: Bimodal character of cyclone climatology in Bay of Bengal modulated by monsoon seasonal cycle, *J. Climate*, **26** (3), 1033-1046.
11. Wu, Liang, Z. Wen, T. Li, and R. Huang, 2014: ENSO-phase dependent TD and MRG wave activity in the western North Pacific. *Climate Dynamics*, 42, 1217-1227.
12. Xu, Y.-M., T. Li, and M. Peng, 2013: Tropical Cyclogenesis in the Western North Pacific as Revealed by the 2008-2009 YOTC data. *Wea. Forecasting*, 28, 1038-1056.
13. Gao, J., and T. Li, 2012: Interannual variation of multiple tropical cyclone events in the western north Pacific, *Advances Atmos.* Sci., **29** (6), 1279-1291
14. Ge, X., T. Li, and M. Peng, 2012: Tropical cyclone genesis efficiency: mid-level versus bottom vortex. *J. Tropical* Meteorology, 19(3), 197-213.
15. Li, T. 2012: Synoptic and climatic aspects of tropical cyclogenesis in Western North Pacific. *Nova Science Publishers*, Inc., Eds. K. Oouchi and H. Fudeyasu, Chap.3, pp.61-94.
16. Hong, C.-C. Y.-H. Li, T. Li , and M.-Y. Lee, 2011: Impacts of Central Pacific and Eastern Pacific El Niños on tropical cyclone tracks over the western North Pacific. *Geophysical Research Letters*, 38, L16712, doi:10.1029/2011GL048821.
17. Gao, J.-Y., and T. Li, 2011: Factors controlling multiple tropical cyclone events in the western North Pacific. *Mon.Wea.Rev.*, 139, 885-894.
18. Zhou, X., B. Wang, X. Ge, and T. Li, 2011: Impact of secondary eyewall heating on tropical cyclone intensity change during eyewall replacement. *J.Atmos.Sci.*, 68, 450–456
19. Hsu, P.C., T. Li, and C.-H. Tsou, 2011: Interactions between boreal summer intraseasonal oscillations and synoptic-scale disturbances over the western North Pacific. Part I: Energetics diagnosis. *J. Climate*, 24, 927-941.
20. Hsu, P.C., and T. Li, 2011: Interactions between boreal summer intraseasonal oscillations and synoptic-scale disturbances over the western North Pacific. Part II: Apparent heat and moisture sources and eddy momentum transport. *J. Climate*, 24, 942-961.
21. Li, T., M. Kwon, M. Zhao, J. Kug, J. Luo, and W. Yu (2010), Global warming shifts Pacific tropical cyclone location, *Geophys. Res. Lett.*, 37, L21804, doi:10.1029/2010GL045124.

22. Zhou, C. and T. Li, 2010: Upscale feedback of tropical synoptic variability to intraseasonal oscillations through the nonlinear rectification of the surface latent heat flux. *J. Climate*, 23, 5738-5754.
23. Chen, J.-M., T. Li, and C.-F. Shih, 2010: Tropical Cyclone and Monsoon Induced Rainfall Variability in Taiwan. *J. Climate*, 23, 4107-4120.
24. Hendricks, E.A., M. S. Peng, B. Fu, and T. Li, 2010: Quantifying environmental control on tropical cyclone intensity change. *Mon.Wea.Rev.*, 138, 3243-3271.
25. Ge, X., T. Li, S. Zhang, and M. Peng, 2010: What causes the extremely heavy rainfall in Taiwan during Typhoon Morakot (2009)? *Atmospheric Science Letters*, 11(1), 46-50.
26. Li, T., 2010: Monsoon climate variabilities. in Climate Dynamics: Why Does Climate Vary?", *Geophys. Monogr. Ser.*, Editor: D.-Z. Sun & B. Frank, doi:10.1029/2008GM000782.
27. Ge, X., T. Li, and M. Peng, 2010: Cyclogenesis simulation of Typhoon Prapiroon (2000) associated with Rossby wave energy dispersion. *Mon.Wea.Rev.*, 138, 42-54.
28. Peng , J., T. Li, M. Peng, and X. Ge, 2009: Barotropic instability in the tropical cyclone outer region. *Quart. J. Roy. Meteor. Soc.*, 135, 851-864.
29. Peng, J., T. Li, and M. Peng, 2009: Formation of tropical cyclone concentric eyewalls by wave-mean flow interactions. *Advances in Geosciences*, Vol. 10, ISBN: 978-981-283-611-3.

Manuscripts submitted:

Bi, M.-Y., T. Li, M. Peng, and X. Shen, 2014: Interaction between Typhoon Megi (2010) and a Low-frequency Monsoon Gyre. submitted to *J. Atmos. Sci.*
Bi, M.-Y., T. Li, M. Peng, and X. Shen, 2014: To What Extent the Presence of Real-Strength Tropical Cyclones Influences the Estimation of Atmospheric Intraseasonal Oscillation Intensity? submitted to *Atmospheric Science Letters*.
Cao, X., T. Li, M. Peng, W. Chen, and G. Chen, 2014: Effects of the monsoon trough intraseasonal oscillation on tropical cyclogenesis over the western North Pacific. *J. Atmos. Sci.*, in revision.